



HAL
open science

Micrometric patterning of a borogermanate glass containing terbium by thermal poling to manage luminescence and second order optical properties

Juliane Resges Orives, Lia Mara Marcondes, Lara Karam, Frédéric Adamietz, Thierry Cardinal, Marc Dussauze, Marcelo Nalin

► To cite this version:

Juliane Resges Orives, Lia Mara Marcondes, Lara Karam, Frédéric Adamietz, Thierry Cardinal, et al.. Micrometric patterning of a borogermanate glass containing terbium by thermal poling to manage luminescence and second order optical properties. *Journal of Physics: Materials*, 2024, 7 (3), pp.03LT01. 10.1088/2515-7639/ad4ba0 . hal-04608517

HAL Id: hal-04608517

<https://hal.science/hal-04608517>

Submitted on 11 Jun 2024

HAL is a multi-disciplinary open access archive for the deposit and dissemination of scientific research documents, whether they are published or not. The documents may come from teaching and research institutions in France or abroad, or from public or private research centers.

L'archive ouverte pluridisciplinaire **HAL**, est destinée au dépôt et à la diffusion de documents scientifiques de niveau recherche, publiés ou non, émanant des établissements d'enseignement et de recherche français ou étrangers, des laboratoires publics ou privés.



Distributed under a Creative Commons Attribution - NoDerivatives 4.0 International License

LETTER • OPEN ACCESS

Micrometric patterning of a borogermanate glass containing terbium by thermal poling to manage luminescence and second order optical properties

To cite this article: Juliane Resges Orives *et al* 2024 *J. Phys. Mater.* 7 03LT01

View the [article online](#) for updates and enhancements.

You may also like

- [Electrochemical Deposition of Terbium from Molten Salts](#)
Sanjeev Rayaprolu and Dev Chidambaram
- [Promoting future sustainable utilization of rare earth elements for efficient lighting technologies](#)
Chen Zhong, Yong Geng, Zewen Ge *et al.*
- [Optical properties of ZnO:SiO₂:Tb³⁺ films: the effect of DNA](#)
E A Boruleva, G K Chudinova, I A Hayrullina *et al.*



The Electrochemical Society

Advancing solid state & electrochemical science & technology

DISCOVER
how sustainability
intersects with
electrochemistry & solid
state science research





LETTER

OPEN ACCESS


RECEIVED
26 October 2023REVISED
11 April 2024ACCEPTED FOR PUBLICATION
14 May 2024PUBLISHED
31 May 2024

Original content from this work may be used under the terms of the [Creative Commons Attribution 4.0 licence](#).

Any further distribution of this work must maintain attribution to the author(s) and the title of the work, journal citation and DOI.



Micrometric patterning of a borogermanate glass containing terbium by thermal poling to manage luminescence and second order optical properties

Juliane Resges Orives^{1,*} , Lia Mara Marcondes³, Lara Karam², Frédéric Adamietz², Thierry Cardinal³, Marc Dussauze^{2,*} and Marcelo Nalin¹

¹ Institute of Chemistry, São Paulo State University (UNESP) —, Araraquara, SP, Brazil

² Institut des Sciences Moléculaires, UMR 5255, Université de Bordeaux, 351 cours de la Liberation, 33405 Talence Cedex, France

³ Institut de Chimie de la Matière Condensée de Bordeaux, Université de Bordeaux, 87 Avenue du Dr Schweitzer, F-33608 Pessac, France

* Authors to whom any correspondence should be addressed.

E-mail: juliane_resges@hotmail.com and marc.dussauze@u-bordeaux.fr

Keywords: thermo-electrical imprinting, control of oxidation, multifunctional glassy material

Abstract

Borogermanate glasses containing terbium ions are interesting materials due to their luminescent and magnetic properties. Terbium can present two different oxidation states and the thermal poling technique can be a pertinent way to modulate spatially the oxidation state of these ions. In this work, we demonstrate using a thermo-electrical imprinting process the transfer of micro scaled motifs on the surface of a borogermanate glass containing Tb³⁺ resulting in a micrometric structuring of the oxidation state of Tb³⁺/Tb⁴⁺ ions. A large change in absorption and luminescence optical properties is observed, arising from the distinct properties of trivalent and tetravalent terbium ions. Correlative micro luminescence, Raman and second harmonic generation measurements were carried out on the patterned poled glass surface. This has demonstrated an accurate concomitant modification of the glass structure accompanying large luminescence changes and the appearance of a second order optical response which could be attributed to a localized space charge implantation. These original results demonstrate how a simple electrical process allows managing multi optical properties but also paves the way to induce static electrical functionalities in a magnetic optical glassy system.

1. Introduction

Designing new materials for which various optical properties are manageable at micrometric scales can lead to new applications in various fields of photonics. As an example, for integrated photonic circuits (PICS) the large variety of devices being developed constantly requires the merging of multiple optical functionalities, including diffractive elements, non-linear responses, and efficient light emission management, among others [1–6].

Among the wide range of materials available for the manufacture of PICS, glasses stand out due to the versatility of their compositions, as well as their simple and low-cost preparation. In addition, glasses are great hosts for rare-earth (RE) ions, which favors the search for luminescent materials with improved optical properties [5–7]. Borogermanate glasses containing Tb³⁺ ions have been investigated in recent years and their potential for photonics and magneto-optical devices have been highlighted [8–13]. Indeed, they are interesting materials due to their luminescent and magnetic properties emerging from the partially filled 4f electronic configurations of terbium [8–10].

The most stable oxidation state of terbium ions is trivalent, but terbium can also present the tetravalent state, having a standard Tb⁴⁺/Tb³⁺ reduction potential of +3.1 V [14, 15]. Regarding the particularities of these two oxidation states, Tb³⁺ has a 4f⁸ electronic configuration, while Tb⁴⁺ is 4f⁷ and the effective magnetic moment for Tb³⁺ and Tb⁴⁺ ions are 9.72 μ B and 7.94 μ B, respectively [1, 16]. In addition, Tb³⁺

ion exhibits its green emission near 544 nm due to the $^5D_4 \rightarrow ^7F_5$ transition, while the Tb^{4+} ions do not exhibit emission and due to its absorption band in the visible region it acts as a quenching center [15, 17].

Some glasses may show coexistence between Tb^{3+}/Tb^{4+} and the existence of this ratio may depend on the oxidation-reduction conditions of the melt or on the oxide concentrations of the matrix [12, 18–20]. Knowing that in glasses, terbium can present two different oxidation states influencing structural, luminescent, optical, and magnetic properties, this opens up opportunities for finding a way to control and/or modulate spatially the oxidation state of terbium.

A technique that has been effectively used for surface modification is thermal poling, which allows modulating different properties in various types of glasses [5, 21–30]. The glass surface modification of the surface consists of heating a glass matrix followed by the application of a high DC voltage for a certain time, during which dissociation processes of ionic charge carriers, commonly alkaline and alkaline earth cations, occurs at the anodic interface [21, 31–33]. It induces both (i) a cationic depletion layer forming a new glassy composition at the anodic surface and (ii) the implantation of a strong static electric field linked to a space charge formed within a layer ranging from a few nanometers to a few micrometers in thickness depending on the parameters used [5, 34–36]. Once this process is carried out, the temperature is decreased to ambient, thus freezing the polarized state on the poled surface.

Over the years, this technique has been improved employing a structured anodic electrode to modify the surface in a patterned way with spatial resolutions on the micrometric scale. This transfer of micro-structured motifs allows controlling several properties, such as chemical reactivity [37], surface durability [38], surface topology [22], surface electrical potential [39]. With regard to optical properties, it is possible to induce a second-order response [5, 40], to prepare waveguides [41], micro-lenses with gradient of refractive index [4] and diffraction gratings [35, 42].

In addition, Lipovskii *et al* showed the possibility of using poling to oxidize Ag and Cu metallic nanoparticles to create optical structures with transparent and colored zones with different absorptions [34, 43]. Recently, thermal poling has been used for the electric field manipulation of magnetic and Faraday rotation performances of a diamagnetic glass, which is of great interest for spintronics devices [44].

Although poling has already been used for several purposes, it has not yet been explored to modulate the properties of rare earth ions. In this context, we focus our attention on demonstrating the control of the oxidation state of terbium ions induced by the thermo-electrical imprinting treatment. Raman, luminescence and second harmonic generation (SHG) correlative imaging are used to show, respectively, the structural modifications, spatial micrometric control of luminescence and second order optical properties on the patterned glass surface.

2. Methods

Borogermanate- Tb^{3+} glasses with a molar composition of $96(46GeO_2-29B_2O_3-16Na_2O-5BaO-4Al_2O_3)-4Tb_4O_7$ was prepared by the melt-quenching method, which consists of melting of precursor components at 1400 °C for 2 h in a platinum crucible followed by quenching into a stainless-steel mold preheated at 450 °C and annealed for 2 h [9]. This composition was chosen due to its high sodium concentration, which is important for the poling process, and because it contains terbium ions, making it possible to study the oxidation of rare earth ions during this process. This pristine glass was labeled as BGTb.

Figure 1(a) illustrates the thermo-electrical imprinting process that was performed in a sealed enclosure under an N_2 flow of 6 l min^{-1} . A piece of silicon wafer was used as cathode and a borosilicate slide was placed between the silicon and the sample as a sacrificial layer in order to preserve the optical quality of the sample at the cathode.

The anode configuration used to pattern the surface was a 100 nm thick platinum film deposited on a silicate glass slide of 25 mm^2 , prepared by a classical lithography process resulting in non-conductive squared motifs of $40 \times 40\ \mu\text{m}^2$ delimited by $10\ \mu\text{m}$ width electrically conductive Pt grid (figure 1(b)). A second electrode of the same size with a homogeneous platinum film was also used. Glass samples were heated up to 300 °C and a DC voltage of 1 kV was applied (at a 300 V min^{-1} rate) and left at these conditions for 30 min. Then, the system was decreased to room temperature and finally the external voltage was removed. The poled samples using the structured and the homogeneous electrode were labeled BGTb-S and BGTb-H, respectively.

After thermal poling treatment, the absorption spectra for BGTb and BGTb-H were obtained between 200 and 800 nm using a double beam Agilent Cary 5000 spectrophotometer. Micro-luminescence data was acquired for BGTb-S using a Labram (Horiba) spectrometer with a laser source at 488 cm^{-1} , a $150\text{ grooves cm}^{-1}$ grating and $50\times$ (N.A. = 0.54) objective. In this configuration, the efficient signal of luminescence allows mapping for large areas (above 0.1 mm^2) to determine the spatial reproducibility of the imprinting process. Then, correlative Raman, luminescence and SHG maps were acquired for the same

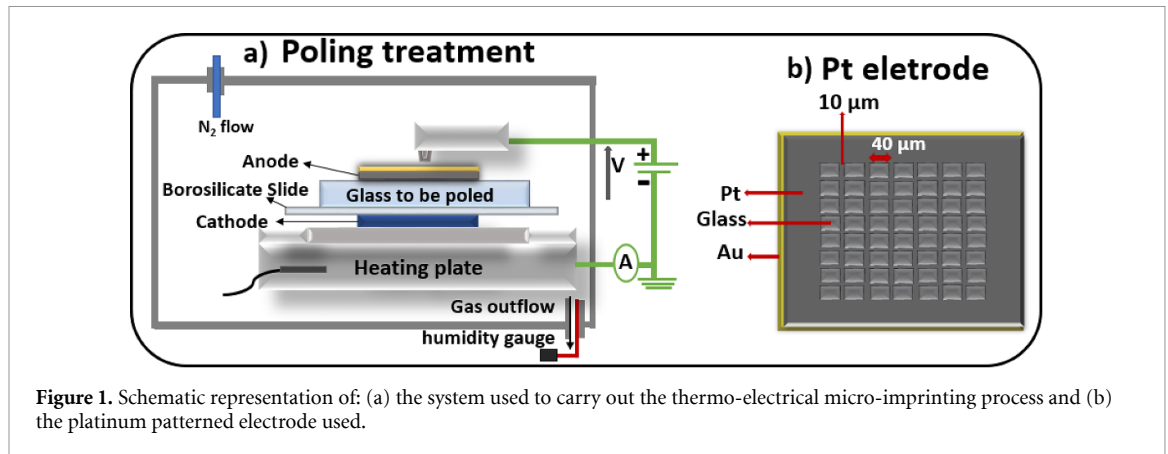


Figure 1. Schematic representation of: (a) the system used to carry out the thermo-electrical micro-imprinting process and (b) the platinum patterned electrode used.

imprinted motif. It consists of a modified confocal micro-Raman spectrometer HR800 (Horiba/Jobin Yvon) with a $100\times$ (N.A. = 0.9) objective. A CW laser operating at 532 nm was used for Raman and luminescence and a picosecond pulsed laser at 1064 nm was used for SHG. All measurements were done in backscattering mode. For the SHG measurements, the incident laser polarization and the analyzed SHG signal polarization states can be linearly polarized either vertically or horizontally.

3. Results and discussion

The BGTb glass obtained by melting quenching is colorless, while the BGTb-S sample after poling treatment showed a change in color to yellow only in the area located under the structured electrode as seen in figure 2(a).

This color change may indicate that an oxidation process from Tb^{3+} to Tb^{4+} occurred as reported for calcium aluminosilicate and borogermanate glasses containing Tb^{3+} [12, 19]. In figure 2(b) we can see by optical microscopy that the imprinting process resulted in a very precise pattern, reproducing the electrode geometry on the glass surface.

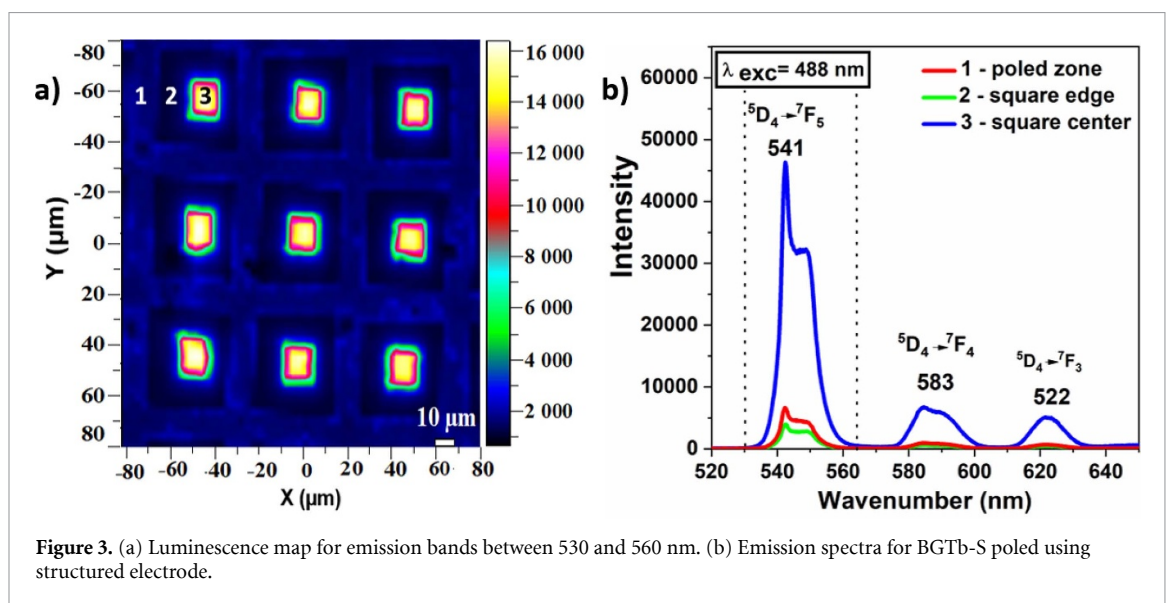
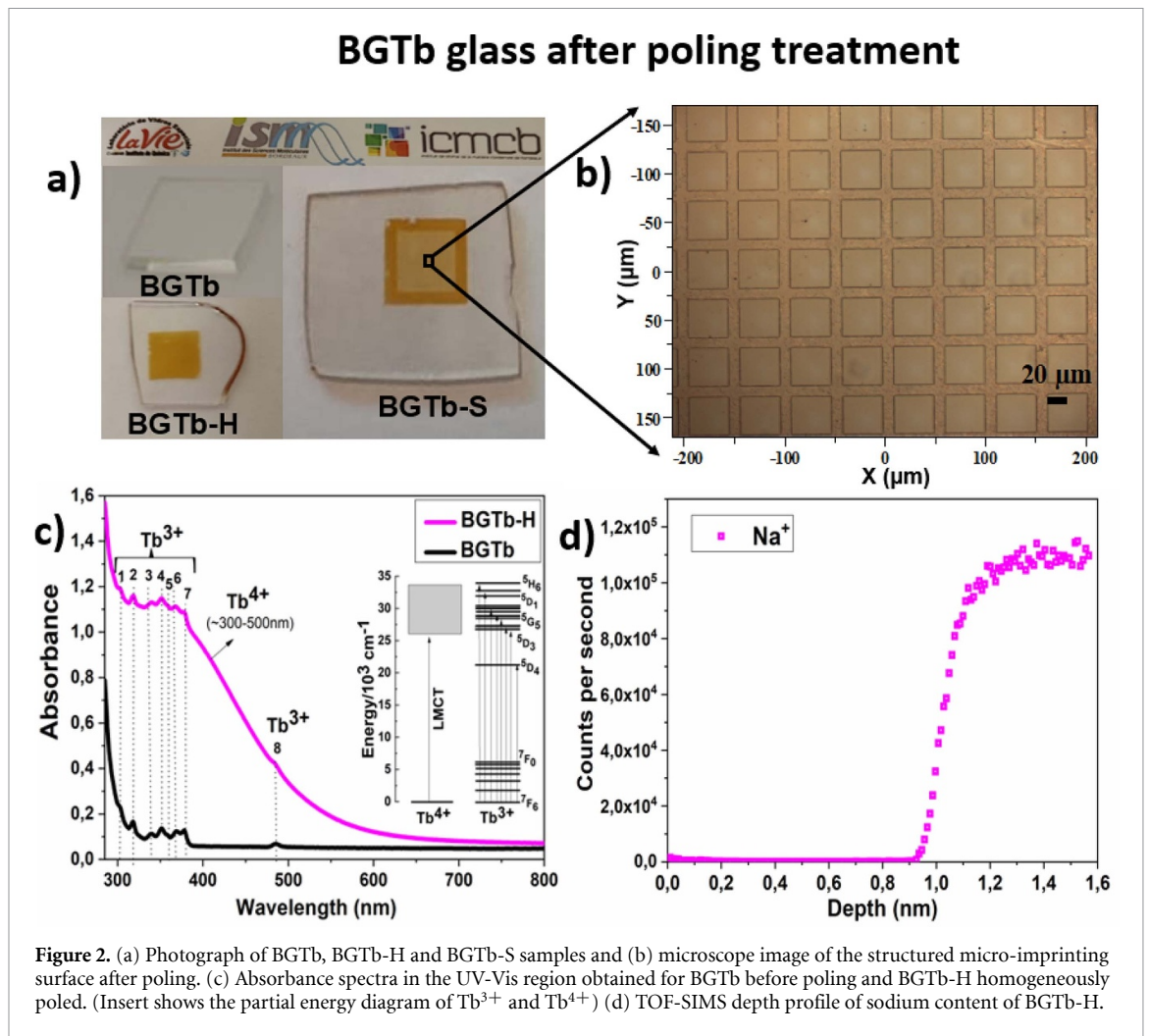
The optical absorption spectra of samples BGTb and BGTb-H are shown in figure 2(c). The recorded absorption bands centered at 302 (1), 318 (2), 340 (3), 350 (4), 358 (5), 370 (6), 378 (7), and 488 (8) nm were assigned to $4f-4f$ transitions from the 7F_6 ground state of Tb^{3+} to the excited levels of 5H_6 , (${}^5D_{0,1}$, 5H_7), (5G_2 , 5L_6), (5L_9 , 5G_4), 5G_5 , ${}^5L_{10}$, (5D_3 , 5G_6), and 5D_4 , respectively [9, 10, 45]. Looking at the absorption of the poled region in the BGTb-H, there is a large absorption between 300 and 500 nm which is assigned to the Tb^{4+} ions electronic transitions from ligand-to-metal charge transfer states coming from one molecular orbital of the oxygen to one f -state of terbium [46, 47]. This broadband covers the blue visible region and gives the sample a yellow color exactly in the poled area and confirms the oxidation of Tb^{3+} ions during the poling process.

In addition to this broad band, it is also possible to notice the absorption band Tb^{3+} as observed for the pristine glass, this occurs because the absorption spectrum is collected for the entire thickness of the sample (0.6 mm) while the glass matrix containing Tb^{4+} is supposed to correspond to the sodium depletion layer which have been measured around $1\ \mu m$ by time-of-flight secondary ion mass spectrometry (ToF-SIMS) as depicted in figure 2(d). Within this polarized layer, the oxidation of terbium ions is supposed to contribute to the compensation of the positive charge (Na^+) displacement.

For the BGTb-S sample, a micro-luminescence mapping was performed in a $160 \times 160\ \mu m^2$ area using for excitation a 488 nm wavelength. The map was generated for emission bands between 530 and 560 nm (figure 3(a)). Due to the fact that Tb^{3+} ions present green emission at 541 nm, while the Tb^{4+} ions have no emission [15, 17], a very contrasted luminescence pattern with a reproducible spatial distribution was created after poling treatment.

Three luminescence spectra (figure 3(b)) were extracted from the map (region 1–3) and shows the bands at 541, 582, and 620 nm assigned to the characteristic transitions of Tb^{3+} ions from 5D_4 to 7F_j ($j = 5, 4, 3$) [9]. In the poled zone (region 1) and the borders of the square (region 2) we observe a decrease in the luminescence intensity of 86% and 92% as compared to the center of the square (region 3), where the luminescence was not affected by the poling treatment.

Indeed, the thermal poling allows forming a controlled oxidation layer in a patterned way under the glass surface in contact with the anode and around the square motifs. We have calculated the emission decrease expected if a complete oxidation of Tb^{3+} is induced within a one micron thick polarized layer by taking in to



account the focal volume and the induced absorption for both the excitation and the back scattered emission. To this aim, if we assume (i) the same laser intensity for all measurements, (ii) no refractive index change between the pristine glass and the poled sample and (iii) a complete oxidation of Tb³⁺ within a layer of thickness $L = 1 \mu\text{m}$ at the anode surface inducing within this layer a complete loss of emission and additional

absorptions at both excitation (488 nm) and emission wavelengths (521 nm), we can estimate the ratio of emission intensities between the pristine glass and the poled glass (BGTb-H) using this equation:

$$\frac{I_{\text{emission}}(\text{pristine glass})}{I_{\text{emission}}(\text{poled glass})} = \frac{Dof}{Dof - L} \times 10^{\text{Abs}(488 \text{ nm})} \times 10^{\text{Abs}(521 \text{ nm})} \quad (1)$$

where Dof is the depth of focus calculated for a numerical aperture of 0.54, L the thickness of the sodium depletion layer (1 μm as shown in figure 2(d)) and $\text{Abs}(521 \text{ nm})$ and $\text{Abs}(488 \text{ nm})$ are obtained from the absorbance curve of BGTb-H depicted from figure 1(c).

An emission decrease of 85% has been estimated corresponding well with the luminescence variations reported in figure 3. It denotes that this poling process could induce locally up to a complete oxidation of Tb ions and this first estimation will be subjected to XPS analysis in a future set of experiments.

The structural changes were evaluated using Raman spectroscopy. Figure 4(a) shows spectra acquired for the poled zone, square center and pristine glass surfaces. The spectra were normalized in intensity at 515 cm^{-1} , corresponding to the $\text{Ge}^{[4]}-\text{O}-\text{Ge}^{[4]}$ vibrational modes of a fully interconnected germanate network [48, 49].

The stretching modes at high frequency are almost inactive for a GeO_2 glass, but they can be observed due to the presence of non-bridging oxygen attributed to the band at 838 cm^{-1} for $(\text{Ge}\emptyset_3\text{O})^-$ structural units stabilized by Na^+ (where \emptyset and O represent bridging and non-bridging oxygen respectively) [49, 50]. This is also due to the presence of a mixture of glass formers for the shoulder at 780 cm^{-1} linked to asymmetric stretching of Ge–O–B bridges [49, 51]. The intensity of the Raman band at 838 cm^{-1} is sensitive to the thermal poling and a decrease is observed indicating a polymerization of the germanate network in the poled layer compensating the excess of negative charge after sodium departure.

The restructuring of $\text{Ge}-\text{O}^-$ terminal bonds into $\text{Ge}-\text{O}-\text{Ge}$ results in the formation of trapped molecular oxygen in the polarized glassy matrix that presents a stretching mode at 1551 cm^{-1} [52]. The presence of O_2 trapped in the poled glass was observed in several poled ionic glasses and is a result of charge compensation mechanisms linked to the structural rearrangement of the glassy matrix [25, 35, 53]. The bands between 1200 and 1500 cm^{-1} are related to borate triangular units vibrations [54–56]. It is also possible to observe a shoulder around 930 cm^{-1} due to vibrational modes of borate tetrahedral units [56]. Structural rearrangements of $[\text{B}\emptyset_4]^-$ units due to the cation migration are not ruled out, but they were not detected by Raman.

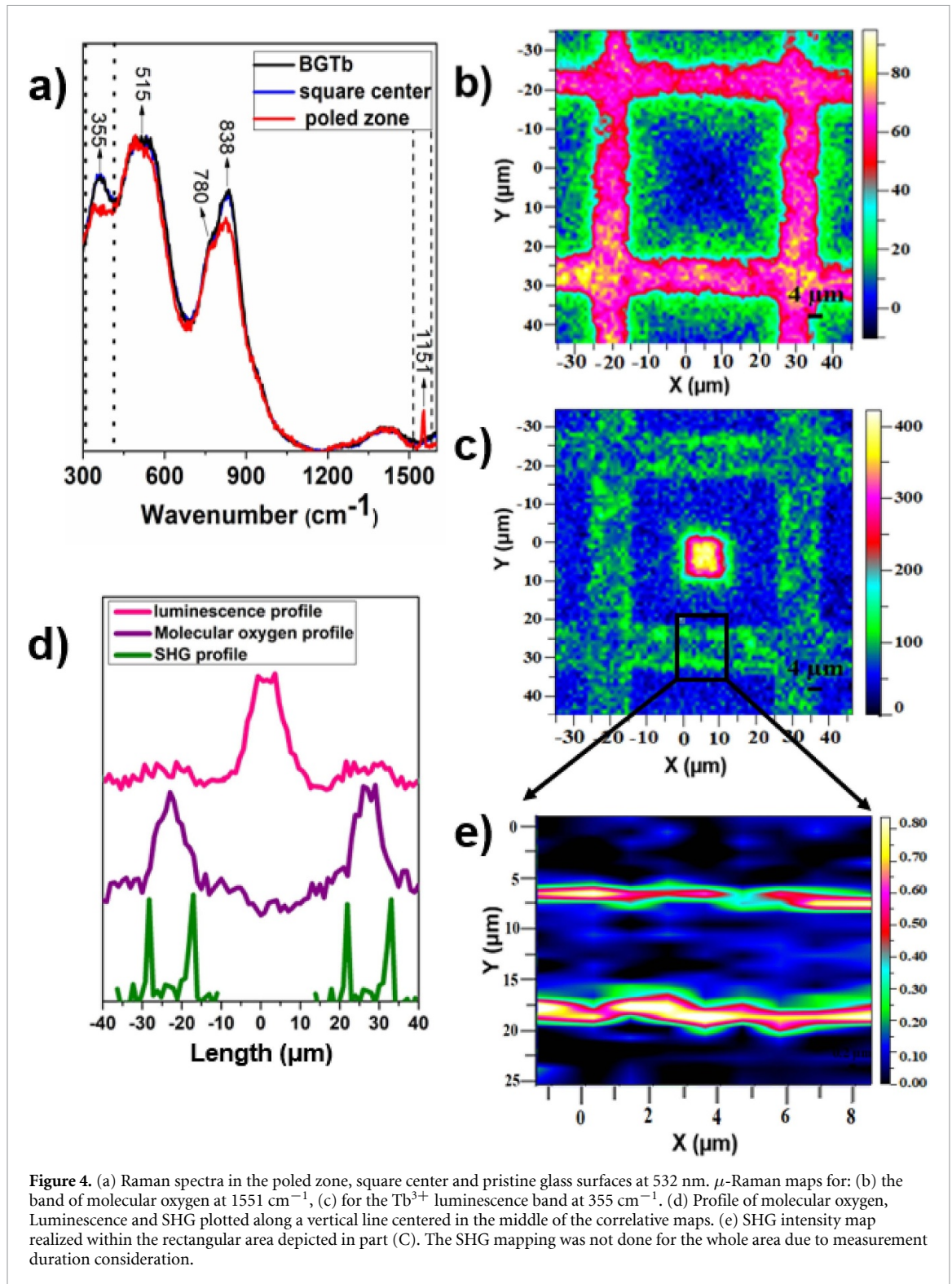
Micro-Raman mapping experiments were carried out in order to follow the spatial locations of structural changes, and an area of $80 \times 80 \mu\text{m}^2$ was mapped. The mapping for the band at 1551 cm^{-1} in figure 4(b) shows the formation of molecular oxygen under the contact zone with the conductive parts of the electrode. As the formation of O_2 is directly related to the restructuring of the network, the mapping of this band tracks the region where the sodium departure occurred, and shows the imprinting accuracy related to compositional and structural glass variations.

For an excitation at 532 nm, in addition to the Raman response of the glass network, a contribution from the luminescence emission of Tb^{3+} ions can be measured. This contribution corresponds to the $^5\text{D}_4$ to $^7\text{F}_5$ transition and is observed at 541 nm or 355 cm^{-1} in Raman shift. Taking advantage of this, we used the same set of data to correlate the Raman and the luminescence signals and thus to spatially correlate structural rearrangements with the oxidation of Tb^{3+} within the same imprinted pattern. In figure 4(c), the image corresponding to the integration of the band at 355 cm^{-1} in Raman shift depicts exactly the same spatial information as that for a luminescence excited at 488 nm as reported in figure 3(a), confirming that our correlative Raman/Luminescence approach is suitable.

Such accurate spatial correlation allows us to observe that for Raman mapping, in the contact zone with the electrode there is the highest concentration of molecular oxygen. This is followed by a gradient at the square edges until it reaches the center where no O_2 can be detected (profile depicted in figure 4(d)).

To explain such spatial gradient, one should consider that the amount of O_2 trapped in the poled glass matrix probed by Raman gives an indication on the oxidation mechanism of the glass matrix occurring during the sodium layer depletion. This signal varies mainly as a function of the polarized layer thickness, which is supposed to be maximum within the zone in direct contact with the electrode (highest local applied voltage) and decreases gradually from the edges of the electrode toward the center of the square motif.

Differently, looking at the luminescence map we do not observe a simple gradient, there is a high luminescence in the center, almost no luminescence at the edges and a slight increase in the zone which was in direct contact with the electrode (luminescence profile provided in figure 4(d)). Finally, one cannot explain the luminescence spatial distribution with a simple variation of local potential linked to the electrode geometry as observed for the O_2 distribution, i.e. for the oxidation of the glass matrix upon the sodium dissociation/depletion process.



The reason why the Tb^{3+} oxidation spatial distribution does not follow simply the local applied voltage during this imprinting process is under investigation and will be reported in a following study including a systematic variation of the poling voltage to determine how both oxidation mechanisms (Tb^{3+} and glass matrix) can be described within a global polarization mechanism adapted for such Terbium rich ionic glassy system.

The effects of the imprinting process on the second order optical response have been mapped by SHG confocal microscopy in reflection mode with steps of 1 μm along X and Y axes (figure 4(e)). The correlative microscopies setup allows probing for the same area structural changes, luminescence and nonlinear optical properties. In the present case, the in-plane SHG components were probed, using the incident beam and the harmonic signal linear and parallel light polarization states.

In figure 4(e), it is possible to observe accurate spatial location of the SHG signal confined at the borders of each imprinted line only if the SHG configuration of polarization is perpendicular to the axis defined by the square pattern. Such an observation is typical for SHG poled patterns in glasses as already reported in the literature [35, 40, 52]. By analogy to these previous reports, one can make the assumption that our observation is linked to an in-plane static field located preferentially at the edges of the electrode breaking the centro symmetry of the glass, inducing a localized second order optical response.

The precise location of the polarization effect on the glass nonlinear optical properties is attributed to an in-plane charge concentration gradient promoted by local field enhancements on the edges of the structured electrode. Such an assumption can also be correlated with the location of the SHG signal within the concentration gradient of trapped O₂ measured by Raman (see SHG and Raman profiles in figure 4(d)).

To sum up the signal intensities coming from μ -luminescence, μ -Raman and μ -SHG measurements are spatially correlated with the electrode's square patterns, showing the accuracy of the thermal poling treatment to modify the surface structurally, to control luminescence at the microscale and to implement localized space charge resulting in second order optical responses.

4. Conclusion

In this work, the control of the oxidation state of terbium ions induced by thermo-electrical imprinting treatment control has been demonstrated. Our present results show that not only has the sodium migration been obtained for classical thermally poled ionic glass, resulting in a sodium-free layer around 1 μ m and molecular oxygen formation at 1551 cm⁻¹, but we also demonstrate the possibility to manage the degree of oxidation of terbium ions upon poling treatment as a charge compensation mechanism for sodium departure.

The oxidation of Tb³⁺ ions to Tb⁴⁺ created a pattern of luminescence signal from high in the region not affected by the polling to low in the region in contact with the electrode due to the Tb⁴⁺ ions not showing luminescence. Furthermore, the sample showed an SHG signal on the edges of the squares patterned on the glass surface. Besides structuring the luminescence properties on a micrometric scale, one should keep in mind that the glass used has magnetic properties, and therefore, the structuring of the magnetic properties is also expected since the magnetic response changes with the oxidation of the Tb³⁺ paramagnetic ions.

Finally, this study opens new perspectives for managing optical functionalities but also strong static electric fields in Terbium rich magnetic glasses, which is a key milestone of progress towards very original multi-functional glassy systems.

Data availability statement

The data cannot be made publicly available upon publication because they are not available in a format that is sufficiently accessible or reusable by other researchers. The data that support the findings of this study are available upon reasonable request from the authors.

Acknowledgments

The authors acknowledge the financial supports from São Paulo Research Foundation Agency, FAPESP (Grant Nos. 2013/07793-6, 2019/19609-1, 2020/15395-4, 2020/01786-1 and 2021/11494-0) and Sistema Nacional de Laboratórios de Fotônica-Ministério da Ciência, Tecnologia e Inovações (SISFOTON-MCTI). The Raman experiments were conducted using the SIV platform at the University of Bordeaux founded by the FEDER and the Region Aquitaine. This project has also received funding from the European Union's Horizon 2020 research program under the Marie Skłodowska Curie Grant Agreement No. 823941 (FUNGLASS), New Aquitaine region (Grant 2016-1R10107) and IDEX Bordeaux (Research Program GPR Light).

Conflict of interest

The authors have no conflicts to disclose.

ORCID iD

Juliane Resges Orives  <https://orcid.org/0000-0002-3950-0040>

References

- [1] Qin J *et al* 2022 *Nanophotonics* **11** 2639
- [2] Syouji A and Tominaga H 2013 *J. Magn. Magn. Mater.* **347** 47
- [3] Liu B, Mo Y, Liu Y, Lu Y, He X, Xu Y, Lipovskii A and Yang G 2022 *Ceram. Int.* **48** 33122
- [4] Lepicard A, Bondu F, Kang M, Sissen L, Yadav A, Adamietz F, Rodriguez V, Richardson K and Dussauze M 2018 *Sci. Rep.* **8** 7388
- [5] Karam L, Adamietz F, Michau D, Murugan G, Cardinal T, Fargin E, Rodriguez V, Richardson K and Dussauze M 2021 *Adv. Photonics Res.* **2** 2000171
- [6] Molina P, Ramirez M O, Garcia-Santizo J V, Alvarez-Garcia S, Pazik R, Strek W, Dereñ P J and Bausá L E 2009 *Appl. Phys. Lett.* **95** 051103
- [7] Wang W and Qi L 2019 *Adv. Funct. Mater.* **29** 1807275
- [8] Gao G, Winterstein-Beckmann A, Surzhenko O, Dubs C, Dellith J, Schmidt M A and Wondraczek L 2015 *Sci. Rep.* **5** 8942
- [9] Franco D F, Fernandes R G, Felix J F, Mastelaro V R, Eckert H, Afonso C R M, Messaddeq Y, Messaddeq S H, Morency S and Nalin M 2021 *J. Mater. Res. Technol.* **11** 312
- [10] Franco D F, Ledemi Y, Correr W, Morency S, Afonso C R M, Messaddeq S H, Messaddeq Y and Nalin M 2021 *Sci. Rep.* **11** 9906
- [11] Guo H, Wang Y, Gong Y, Yin H, Mo Z, Tang Y and Chi L 2016 *J. Alloys Compd.* **686** 635
- [12] Savinkov V I, Sigaev V N, Golubev N V, Sarkisov P D, Masalov A V and Sergeev A P 2010 *J. Non-Cryst. Solids* **356** 1655
- [13] Yin H, Gao Y, Guo H, Wang C and Yang C 2018 *J. Phys. Chem. C* **122** 16894
- [14] Akahoshi D, Hosouchi Y, Inoue R, Kuwahara H and Saito T 2021 *J. Solid State Chem.* **303** 122452
- [15] Kaszewski J, Witkowski B S, Wachnicki L, Przybylińska H, Kozankiewicz B, Mijowska E and Godlewski M 2016 *J. Rare Earth* **34** 774
- [16] Hinatsu Y 1992 *J. Solid State Chem.* **100** 136
- [17] Verma R K, Kumar K and Rai S B 2010 *Solid State Sci.* **12** 1146
- [18] Chen Q, Chen Q, Wang H, Wang G and Yin S 2017 *J. Non-Cryst.* **470** 99
- [19] Sontakke A D and Annapurn K 2012 *Spectrochim. Acta A* **94** 180
- [20] Culea E 2011 *J. Non-Cryst. Solids* **357** 50
- [21] Dussauze M, Cremoux T, Adamietz F, Rodriguez V, Fargin E, Yang G and Cardinal T 2012 *Int. J. Appl. Glass. Sci.* **3** 309
- [22] Karam L, Alvarado R, Calzavara F, Dahmani R, Kang M, Blanco C, Adamietz F, Richardson K and Dussauze M 2022 *Opt. Mater. Express* **12** 1920
- [23] Lepicard A, Adamietz F, Rodriguez V, Richardson K and Dussauze M 2018 *Opt. Mater. Express* **8** 1613
- [24] Raskhodchikov D, Reshetov I, Brunkov P, Kaasik V, Lipovskii A and Tagantsev D 2020 *J. Phys. Chem. B* **124** 7948
- [25] Redkov A V, Melehin V G and Lipovskii A 2015 *J. Phys. Chem. C* **119** 17298
- [26] Dussauze M, Kamitsos E I, Fargin E and Rodriguez V 2007 *J. Phys. Chem. C* **111** 14560
- [27] Galleani G, Abou Khalil A, Canioni L, Dussauze M, Fargin E, Cardinal T and de Camargo A S S 2023 *J. Non-Cryst. Solids* **601** 122054
- [28] Poirier G, Dussauze M, Rodriguez V, Adamietz F, Karam L, Cardinal T and Fargin E 2019 *J. Phys. Chem. C* **123** 26528
- [29] Guimbretiere G, Dussauze M, Rodriguez V and Kamitsos E I 2010 *Appl. Phys. Lett.* **97** 171103
- [30] Nasu H, Ito Y, Yamamoto Y, Hashimoto T and Kamiya K 2001 *J. Ceram. Soc. Japan* **109** 366
- [31] Fleming L A H, Goldie D M and Abdolvand A 2015 *Opt. Mater. Express* **5** 1674
- [32] Quiquempois Y, Godbout N and Lacroix S 2002 *Phys. Rev. A* **65** 043816
- [33] Liu X-M and Zhang M-D 2001 *Jpn. J. Appl. Phys.* **40** 4069
- [34] Lipovskii A A, Melehin V G and Petrikov V D 2006 *Tech. Phys. Lett.* **32** 275
- [35] Dussauze M, Rodriguez V, Adamietz F, Yang G, Bondu F, Lepicard A, Chafer M, Cardinal T and Fargin E 2016 *Adv. Opt. Mater.* **4** 929
- [36] Reduto I, Kamenskii A, Brunkov P, Zhurikhina V, Svirko Y and Lipovskii A 2019 *Opt. Mater. Express* **9** 3059
- [37] Lepicard A, Cardinal T, Fargin E, Adamietz F, Rodriguez V, Richardson K and Dussauze M 2015 *J. Phys. Chem. C* **119** 22999
- [38] Chazot M *et al* 2021 *J. Am. Ceram. Soc.* **104** 157
- [39] Alvarado R *et al* 2020 *J. Phys. Chem. C* **124** 23150
- [40] Karam L *et al* 2020 *Adv. Opt. Mater.* **8** 2000202
- [41] Margulis W and Laurell F 1997 *Appl. Phys. Lett.* **71** 2418
- [42] Kamenskii A N, Reduto I V, Petrikov V D and Lipovskii A A 2016 *Opt. Mater.* **62** 250–4
- [43] Lipovskii A, Kuittinen M, Karvinen P, Leinonen K, Melehin V G, Zhurikhina V V and Svirko Y P 2008 *Nanotechnology* **19** 415304
- [44] Chen Q, Li Z and Chen W 2021 *J. Non-Cryst. Solids* **564** 120850
- [45] Sontakke A D, Biswas K and Annapurna K 2009 *J. Lumin.* **129** 1347
- [46] López-Pacheco G, Padilla-Rosales I, López-Juárez R and González F 2021 *ECS J. Solid State Sci. Technol.* **10** 116007
- [47] Hoefdraad H E 1975 *J. Inorg. Nucl. Chem.* **37** 1917
- [48] McKeown D M and Merzbacher C I 1995 *J. Non-Cryst. Solids* **183** 61
- [49] Zaiter R, Dussauze M, Nalin M, Fargin E, Adamietz F, Danto S, Toulemonde O and Cardinal T 2022 *J. Alloys Compd.* **912** 165181
- [50] Henderson G S, G. Soltay L and Wang H M 2010 *J. Non-Cryst. Solids* **356** 2480
- [51] Skopak T, Kroeker S, Levin K, Dussauze M, Méreau R, Ledemi Y, Cardinal T, Fargin E and Messaddeq Y 2018 *J. Phys. Chem. C* **123** 1370
- [52] Poirier G, Karam L, Rodriguez V, Adamietz F, Cardinal T, Evelyne F and Dussauze M 2022 *J. Mater. Chem. C* **10** 10310
- [53] Cremoux T, Dussauze M, Fargin E, Cardinal T, Talaga D, Adamietz F and Rodriguez V 2014 *J. Phys. Chem. C* **118** 3716
- [54] Sun X-Y, Jiang D-G, Chen S-W, Zheng G-T, Huang S-M, Gu M, Zhang Z-J, Zhao J-T and Ballato J 2013 *J. Am. Ceram. Soc.* **96** 1483
- [55] Koroleva O N, Shtenberg M V, Zainullina R T, Lebedeva S M and Nevolina L A 2019 *Phys. Chem. Chem. Phys.* **21** 12676
- [56] Möncke D, Dussauze M, Kamitsos E I, Varsamis C P E and Ehrtd D 2009 *Phys. Chem. Glasses: Eur. J. Glass Sci. Technol. B* **50** 229 (available at: www.ingentaconnect.com/contentone/sgt/ejgst/2009/00000050/00000003/art00018)